TRANSMIT RADIO-FREQUENCY FIELD MAPPING IN HIGH FIELD MAGNETIC RESONANCE IMAGING

By

Anuj Sharma

Thesis

Submitted to the Faculty of the

Graduate School of Vanderbilt University

in partial fulfillment of the requirements

for the degree of

MASTER OF SCIENCE

in

BIOMEDICAL ENGINEERING

May, 2013

Nashville, Tennessee

Approved:

Professor William A. Grissom

Professor Adam Anderson

ACKNOWLEDGEMENTS

First of all I would like to thank my advisor Dr. William A. Grissom for accepting me as a student in his laboratory two years ago. Since then I have learned a lot under his guidance both professionally and personally. His qualities of unabated enthusiasm and kindness have shown me what a good scientist and a good person should be.

I am grateful to Vanderbilt University Graduate School for awarding me the Tuition Scholarship without which I may not have been able to pursue higher education in the United States. I am also indebted to Dr. Adam Anderson for serving on my committee and for showing me the ropes of MRI during his course on medical imaging.

I am thankful to everyone with whom I had the pleasure of working during the course of this project. Especially I would like to thank my lab mates Pooja and Julianna and all my office neighbours for the fruitful discussions and the cheerful jokes that we share.

None of my work was possible without the constant support of my family. I would like to thank my parents and uncles for encouraging me in all my pursuits. Lastly and most importantly I thank my loving wife Priyanka who has always believed in me and has been unconditionally supportive in all my endeavours in and beyond graduate school. This was not possible without her.

TABLE OF CONTENTS

Page

LIST OF FIGURES

CHAPTER I

INTRODUCTION

This research project focuses on the development of accelerated transmit radio-frequency (RF) field mapping techniques in parallel Magnetic Resonance Imaging (MRI). Specifically it is shown that the Bloch-Siegert (BS) $|B_1^+|$ mapping method [2] can be accelerated using partially parallel auto-calibrating image reconstruction methods such as GRAPPA [3] and SPIRiT [4]. In this chapter, we will review the fundamentals of parallel imaging (PI) and focus on the details of GRAPPA and SPIRiT. We will then discuss the BS method in conjunction with other approaches to field mapping.

I.1 Parallel Imaging

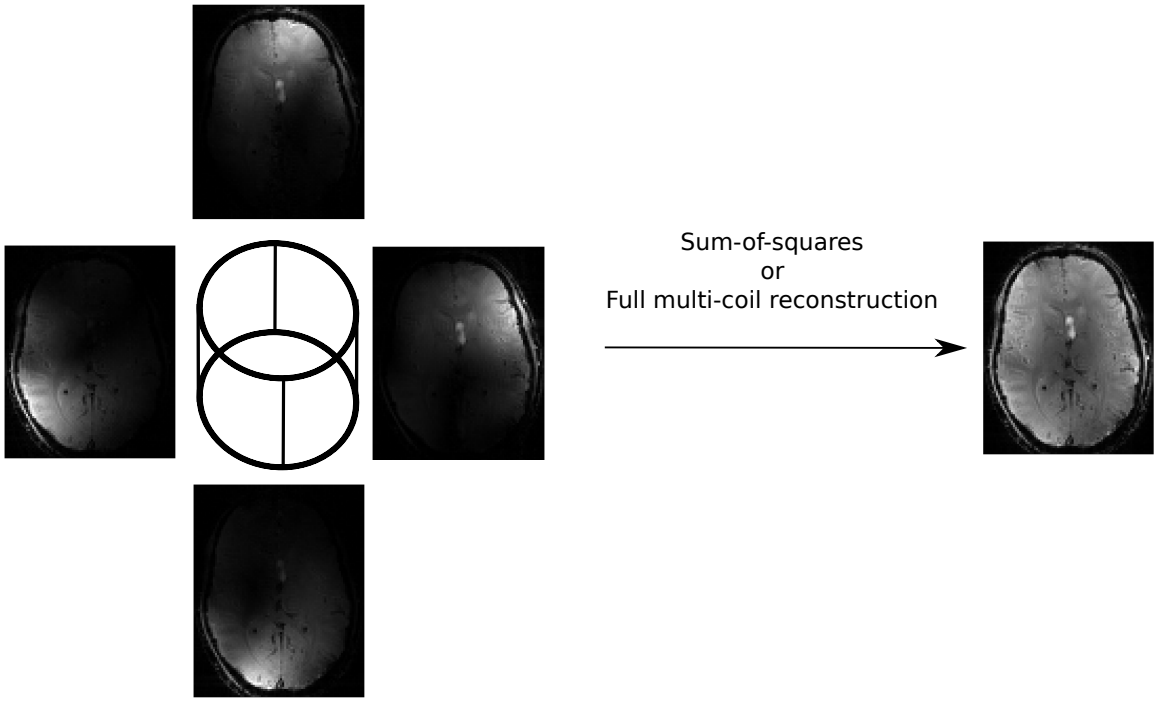

Figure I.1: Parallel imaging makes use of phased array coils. In this example images acquired using a 4 element coil are shown. Coil sensitivities get multiplied with the image and thus provide spatial encoding. The multi-coil images can be combined using sum-of-squares or a full multi-coil reconstruction when the coil sensitivities are known.

In MRI spatial encoding of the signal is achieved by applying spatially varying magnetic fields called the gradient fields. In 2D imaging the location of the signal is resolved along the two dimensions by applying two gradient fields called the frequency encoding and phase encoding gradients. In 3D imaging an additional phase encoding gradient is used to resolve the signal along the third dimension. Of the two encoding steps, phase encoding is the most time consuming. The effect of the phase encoding gradient is to select a single spatial frequency along the phase encode direction. To acquire all spatial frequencies required to reconstruct an image, the phase encode step must be repeated multiple times, with varying phase encoding gradient strength.

Parallel imaging in MRI refers to the use of phased array coils to simultaneously acquire multiple views of the same object. As Figure I.1 shows, the image acquired by each coil is weighted by the coil's sensitivity which are spatially-localized. In practice the image is weighted by the square of the sensitivity, once each for transmit and receive sensitivities. The images from individual coils can be combined using a sum-of-squares or a multi-coil reconstruction which are shown to be SNR optimal in Ref. [5].

An intuitive way to reduce scan time is to reduce the number of phase encoding lines acquired to reconstruct an image with the required fidelity. Increasing the distance between phase encoding lines while not changing the maximal extent of k-space reduces scan time while maintaining the image resolution. As Figure I.2 shows, skipping k-space lines effectively reduces the k-space sampling rate and thus reduces the field of view in the phase encode direction. If the sampling rate violates the Nyquist criteria then aliasing artifacts are seen in the image domain. The goal of all PI methods is to allow large k-space sampling intervals while utilizing the spatial encoding provided by array coils to upsample the signal to the Nyquist rate. PI reconstruction methods can be broadly classified into image based and k-space based methods. Image based methods such as SENSE [6] start with aliased images and unfold the aliasing in the image domain. k-Space based methods such as GRAPPA [3] fill in the missing data in k-space and then apply Fourier transformation to

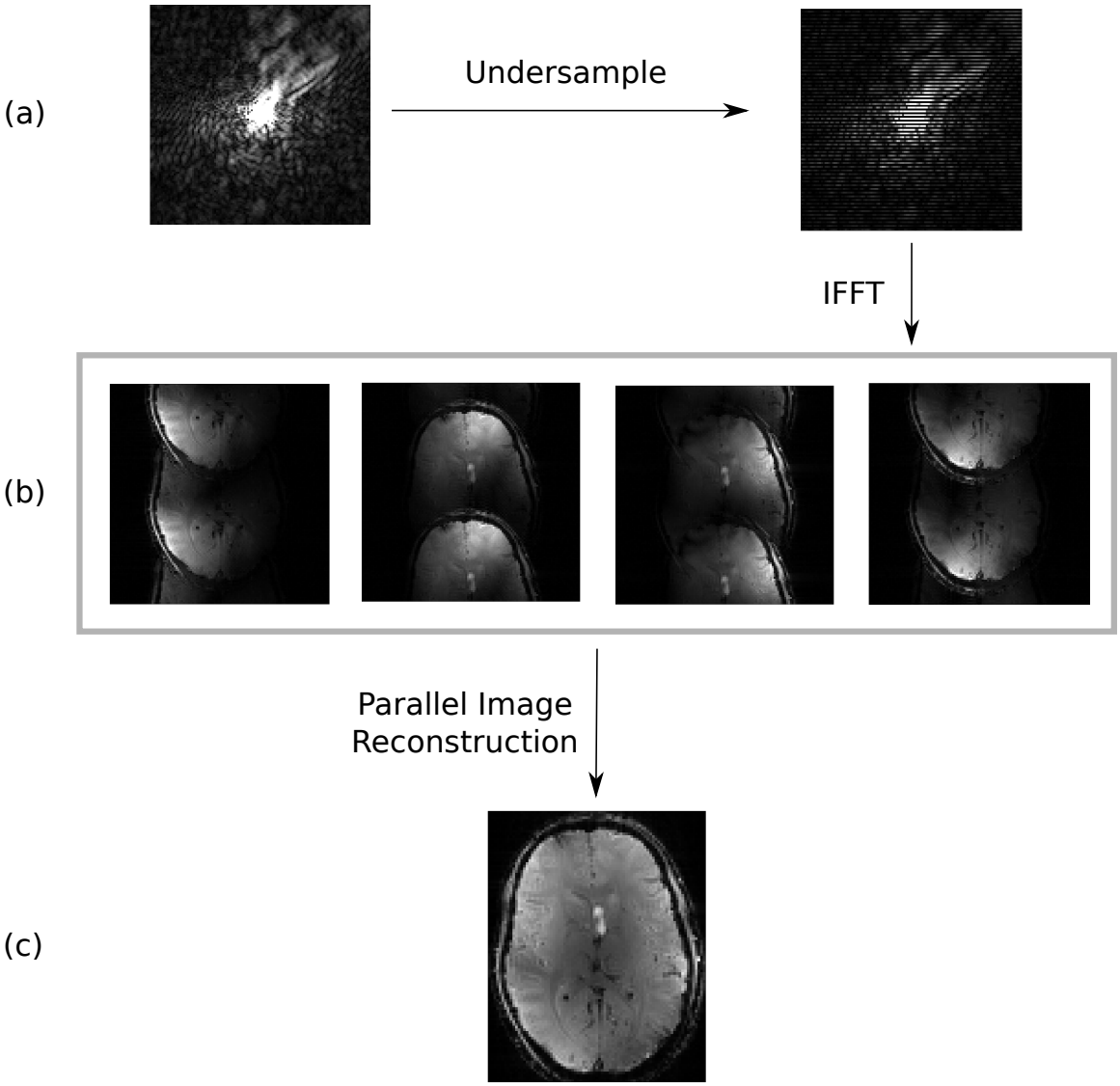

Figure I.2: The goal of all parallel imaging reconstruction methods is to undo the image aliasing caused by decimating k-space data. In this example (a) k-space data is undersampled by a factor of $2\times$ by skipping every alternate TR in a Cartesian scan. (b) Straightforward inverse FFT gives aliasing artifact in the phase encode direction. (c) Parallel imaging reconstruction produces either an unaliased image per coil or a single unaliased image which has contributions from all the coils.

get unaliased images. There are also methods such as SMASH [7] that work in the hybrid space. The data is reconstructed in the k-space while the coil sensitivities are treated in the image space. PI methods also differ in the number of output images. Some methods produce a single coil-combined image and other methods reconstruct one image per coil.

I.1.1 GRAPPA

GRAPPA is a pure k-space based PI method introduced by Griswold et. al. in 2002 [3]. The idea in GRAPPA is to synthesize the unsampled k-space data from a neighbourhood of acquired data points. Unlike image based methods such as SENSE and hybrid-space based methods such as SMASH, GRAPPA does not require the knowledge of coil sensitivity maps. The aim is to calculate weights that relate each unacquired sample to its neighbourhood of acquired data points across all coils. A fully-sampled set of points called the calibration region is typically acquired at the center of k-space. When the calibration region is acquired in the same scan as the accelerated data the samples in the calibration region are called the auto-calibration signal (ACS) lines. The ACS lines are used to calculate the GRAPPA kernel weights. Then each unacquired data point is synthesized from its neighbirhood using the calculated weights.

The process of reconstructing missing data for each coil can be represented as

$$\hat{m_k}(k_x,k_y) = \sum_{i,j,l} a_{i,j,l} m_l(k_x + i\Delta k_x, k_y + j\Delta k_y) \tag{I.1}$$

where $\hat{m_k}$ are the estimates of the missing k-space data for coil k and m_l are the acquired data for coil l at location (k_x,k_y), Δk_x and Δk_y are the k-space sampling steps in x and y directions respectively and i,j index locations of the acquired samples. $a_{i,j,l}$ are the kernel weights and are called the GRAPPA operator. Inside the calibration region the k-space values at all the locations are exactly known so Equation I.1 can be solved for $a_{i,j,l}$. Equation I.1 can be rewritten in matrix-vector form as

$$M_l = a_l M_A \tag{I.2}$$

where, M_l is the calibration data for coil l, M_A is the matrix of acquired samples in a predefined neighbourhood across all coils and a_l are the GRAPPA kernel weights. Equation

I.2 is solved to get an estimate of the GRAPPA operator $\hat{a}_l$

$$\hat{a}_l = (M_A^{'} M_A + \lambda I)^{-1} M_A^{'} M_l \tag{I.3}$$

where λ is a regularization parameter used to improve the conditioning of the problem and I is the identity matrix. The missing data points for each coil are then calculated by applying the GRAPPA operator in their neighbourhood using Equation I.1. The k-space data for each coil is Fourier transformed to get the estimated image for each coil. These images can then be combined using a sum-of-squares reconstruction to produce an unaliased image.

In GRAPPA, the weights in the synthesizing kernel are dependent on the pattern of acquired points in the neighbourhood of each unacquired point. Thus the weights are spatially varying which makes GRAPPA difficult to implement even for simple undersampling patterns. This is illustrated in Figure I.3 for $4\times$ acceleration achieved by skipping phase encode lines in 3D imaging. This challenge is addressed by SPIRiT which we will discuss next.

I.1.2 SPIRiT

This section is based on material from Ref. [4]

Inspired by GRAPPA, Lustig et. al. introduced SPIRiT [4] which is a general framework for parallel image reconstruction that makes use of data more efficiently. In SPIRiT the problem of parallel image reconstruction is formulated as an optimization constrained by data consistency. The constraints are separated into (a) consistency with the calibration and (b) consistency with the data acquisition. While GRAPPA enforces calibration consistency only between synthesized points and acquired points in a close neighbourhood, SPIRiT expands the notion of calibration consistency by including all the points (both acquired and synthesized) in the neighbourhood across all coils. Figure I.3 illustrates how, unlike GRAPPA, the kernel weights in SPIRiT are independent of the sampling pattern at each spatial location.

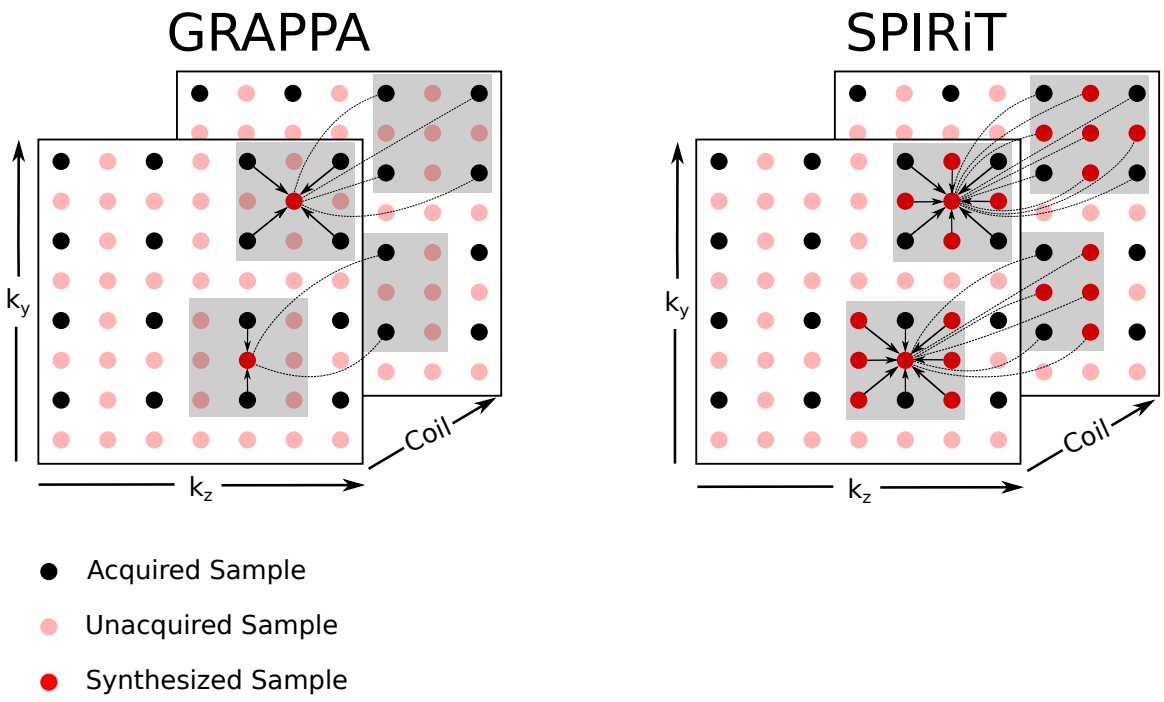

Figure I.3: GRAPPA vs. SPIRiT. (a) In traditional 2D GRAPPA each missing k-space data sample is synthesized from a neighbourhood of acquired points. The GRAPPA kernel is dependent on the pattern of acquired points in the neighbourhood. (b) In SPIRiT, reconstruction of each missing k-space sample is dependent on a neighbourhood of both acquired and skipped points. The kernel is independent of the sampling pattern in the neighbourhood.

If x represents the entire k-space data for all coils, and G is a matrix containing the SPIRiT kernel weights, the calibration consistency constraint is given by

$$x = Gx \tag{I.4}$$

The second constraint of data consistency comes naturally from the fact that the reconstructed data should be consistent with the actual data acquired by the scanner at the sampled locations. This constraint can be represented as

$$y = Dx \tag{I.5}$$

where y is the acquired data and D is a linear operator that relates the reconstructed Cartesian k-space x to the acquired data. The reconstruction is treated as the solution to an optimization problem given by

$$\begin{aligned} &minimize && ||(G-I)x||^2 \\ &s.t. && ||Dx-y||^2 \quad \leq \quad \varepsilon \end{aligned} \tag{I.6}$$

where ε is a constant that trades off data consistency with calibration consistency. This problem can be efficiently solved using iterative descent methods such as steepest descent or the conjugate gradient (CG) method.

In this work we have chosen SPIRiT as the primary auto-calibrating partially parallel image reconstruction method. SPIRiT is a general PI framework that works for both uniform and non-uniform k-space trajectories. We take advantage of this and show that the proposed method is a general approach for both uniform imaging such as Cartesian and non-uniform imaging such as Spiral sampling.

I.2 Transmit RF Field Mapping

In MRI, RF coils are used to interact with molecular species which are typically protons. After the protons are polarized using the main magnetic field (B_0), conventionally along the longitudinal axis, the protons start precessing at a characteristic frequency called the Larmour frequency which is given by

$$\omega = \gamma B_0 \tag{I.7}$$

where γ is the gyromagnetic ratio and has a value of $2\pi \times 42.57$ MHz/T for protons. In MRI jargon the precessing protons are called spins. To generate an MR signal the spins need to be tipped to the transverse plane. To achieve this, a transmit RF coil is used to excite the spins. After excitation, the transmit field is turned off and the spins begin to return to equilibrium magnetization. The rate at which the spins decay is characteristic of

tissue property. The spin decay rate along with pulse sequence timing parameters form the basis of signal contrast in MRI. The excitation phase is followed by signal encoding using the gradient coils, as described in section I.1. When the signal is ready to be acquired the receive RF coils are turned on and the decaying spin magnetization produces an emf in the coils. In practice a single coil could be used for both transmission and reception or multiple coils could be used for transmission and/or reception.

Ideally, the RF coils would have a uniform response, for example, two identical spins at two locations in the field of view would generate the same emf in the receive coil. But in practice, the transmit and receive RF coil sensitivities are a function of space and are represented by $B_1^+(\vec{x})$ and $B_1^-(\vec{x})$ respectively, where $\vec{x}$ is the space variable. The B_1 field can be divide into a right-circularly polarized field (B_1^-) and a left-circularly polarized field (B_1^+). By convention, the left-circularly polarized field rotates in the same direction as the spins, so this component has a larger effect than the right-circularly polarized component which is $2\gamma B_0$ off-resonance and can be ignored.

When an excitation pulse is played on the RF coil, the spins get tipped to the transverse plane by an angle called the flip angle. The flip angle of an on-resonant spin is dependent on the time-dependent RF pulse envelope ($b_1(t)$) and the magnitude of $B_1^+(\vec{x})$, and is given by

$$\theta(\vec{x}) = \gamma \int_0^T |B_1^+(\vec{x})| b_1(t) dt \tag{I.8}$$

From Eq. I.8, if $|B_1^+(\vec{x})|$ is not uniform over space then the flip angle seen by the spins will be different at different locations. This can reduce the image quality by introducing spatially varying image contrast and shading artifacts.

To design methods to correct the adverse effects of non-uniform $|B_1^+|$ fields a map of the $|B_1^+|$ is required. Specifically, $|B_1^+|$ mapping is required in applications such as quantitative imaging, $|B_1^+|$ shimming and parallel transmission. However $|B_1^+|$ mapping is time consuming as it must be performed during pre-scan in each subject, for each transmit coil and over the entire imaging volume. Ideally the fields for each element of an array

could be rapidly measured during a prescan stage over the entire imaging volume, but the measurement time scales with the number of transmit channels, and even the fastest field mapping techniques suffer from relatively long acquisition times for many coils.

$|B_1^+|$ mapping techniques can be broadly classified into two classes: signal phase based and signal magnitude based methods. These methods depend on the change in signal magnitude or phase based on $|B_1^+|$. Magnitude based methods generally suffer from problems such as T_1 dependence and large RF power deposition. These problems are mitigated by phase-based methods. In this work we have used a phase based approach called the Bloch-Siegert method. This method was chosen because it is fast and robust to TR, T_1 relaxation, flip angle, chemical shift, background field inhomogeneity, and magnetization transfer [8].

I.2.1 Double-Angle Method

The Double-Angle mapping [16] is an image magnitude based method to calculate a flip-angle map, which is an indirect measure of the $|B_1^+|$ field. This method is based on the fact that for a given flip angle θ, the image signal in a voxel is proportional to $sin(\theta)$. To calculate the flip angle map, two images I_1 and I_2 are acquired with flip angles θ and 2θ, respectively. If all pulse sequence parameters are kept constant, then the ratio of the magnitude images satisfies

$$\frac{I_2(\vec{x})}{I_1(\vec{x})} = \frac{sin(2\theta(\vec{x}))f_2(T_1,TR)}{sin(\theta(\vec{x}))f_1(T_1,TR)} \tag{I.9}$$

where $\theta(\vec{x})$ represents the spatially varying flip angles due to B_1^+ inhomogeneity and f_1, f_2 are the effects on the image signal due to spin lattice relaxation time (T_1) and choice of pulse repetition time (TR). If the effects of T_1 and spin-spin relaxation time (T_2) are neglected then the flip angle map can be calculated as

$$\theta(\vec{x}) = arccos\left(\left|\frac{I_2(r)}{2I_1(r)}\right|\right) \tag{I.10}$$

In practice, to remove T_1 dependence, TR is set to a value several times higher than T_1. This leads to undesirably long acquisition times, especially for molecular species with high T_1 values. The Double-Angle method also suffers from problems such as due to background field inhomogeneity and chemical shift artifacts, which are typical for magnitude based $|B_1^+|$ mapping methods. Both these limitations are overcome by the Bloch-Siegert method which is discussed next.

I.2.2 Bloch-Siegert Method

Bloch-Siegert $|B_1^+|$ mapping is a phase-based method based on the Bloch-Siegert effect. When an off-resonance RF field is applied to a nucleus, its resonance frequency shifts. This effect is called the Bloch-Siegert shift [9], [10]. When the RF is far enough off-resonance or a pulse shape is chosen such that it does not cause excitation, the spins experience a change in precession frequency without excitation. The shift in precession frequency is dependent on the magnitude of the B_1^+ field and the difference between the spin resonance and RF frequency. Under the assumption that the applied RF is far from off-resonance, the precession shift can be approximately represented as

$$\omega_{BS} = \frac{(\gamma|B_1^+|)^2}{2\omega_{RF}} \tag{I.11}$$

where ω_{BS} is the BS frequency shift, γ is the gyromagnetic ratio, and ω_{RF} is the large frequency offset of the applied RF pulse away from the resonant frequency.

In Ref [8] Sacolick et al. show that for any arbitrary pulse $B_1(t)$ the relationship between the BS phase shift and peak B_1 is given by

$$\begin{aligned} \phi_{BS} &= B_{1,peak}^2 \int_0^T \frac{(\gamma B_{1,normalized}(t))^2}{2\omega_{RF}(t)} dt \\ &= B_{1,peak}^2 \times K_{BS} \end{aligned} \tag{I.12}$$

where, ϕ_{BS} is the BS phase shift, $B_{1,peak}$ is the magnitude of the peak B_1, $B_{1,normalized}(t)$ is

the RF pulse normalized to have a peak magnitude of 1 and K_{BS} is a constant that describes the phase shift in $radians/Gauss^2$ for a given pulse. Note that this is an approximate solution on which the BS method is based. A more detailed derivation is given in Ref. [10].

The method is made more robust by acquiring two scans at symmetric off-resonance frequencies ($+\omega_{RF}$ and $-\omega_{RF}$) around the water peak. The BS phase shift is estimated by taking the phase difference between the two scans. As unwanted phase accrual due to off-resonance effects such as B_0 inhomogeneity and chemical shifts are the same for the two scans, the difference operation removes them.

Figure I.4 shows an illustration of a Gradient Echo (GE) BS $|B_1^+|$ mapping pulse sequence. After exciting the spins with a slice-selective pulse, a Fermi pulse is applied as the BS encoding pulse. The signal is generated as usual in a GE sequence by rephasing the spins using the readout gradient. The BS sequence can be implemented on the scanner with very small changes to the GE sequence. For this work, we used the BS protocol which was implemented by Jankiewicz et al. [11] by modifying the stock Fast Field Echo (FFE) sequence on the Philips 7T human scanner.

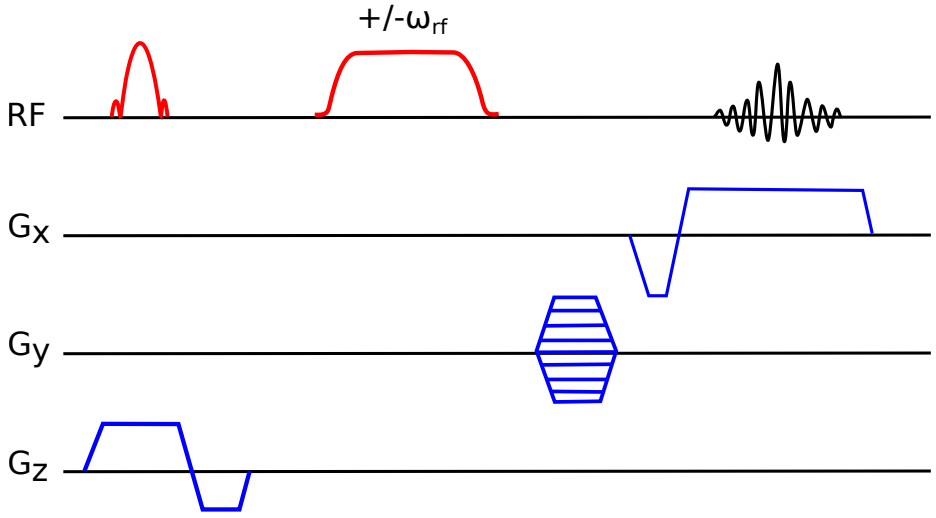

Figure I.4: Gradient echo sequence for Bloch-Siegert $|B_1^+|$ mapping. The BS method can be easily incorporated into a gradient or spin echo sequence.

CHAPTER II

ACCELERATED BLOCH-SIEGERT TRANSMIT RADIO-FREQUENCY FIELD MAPPING

II.1 Introduction

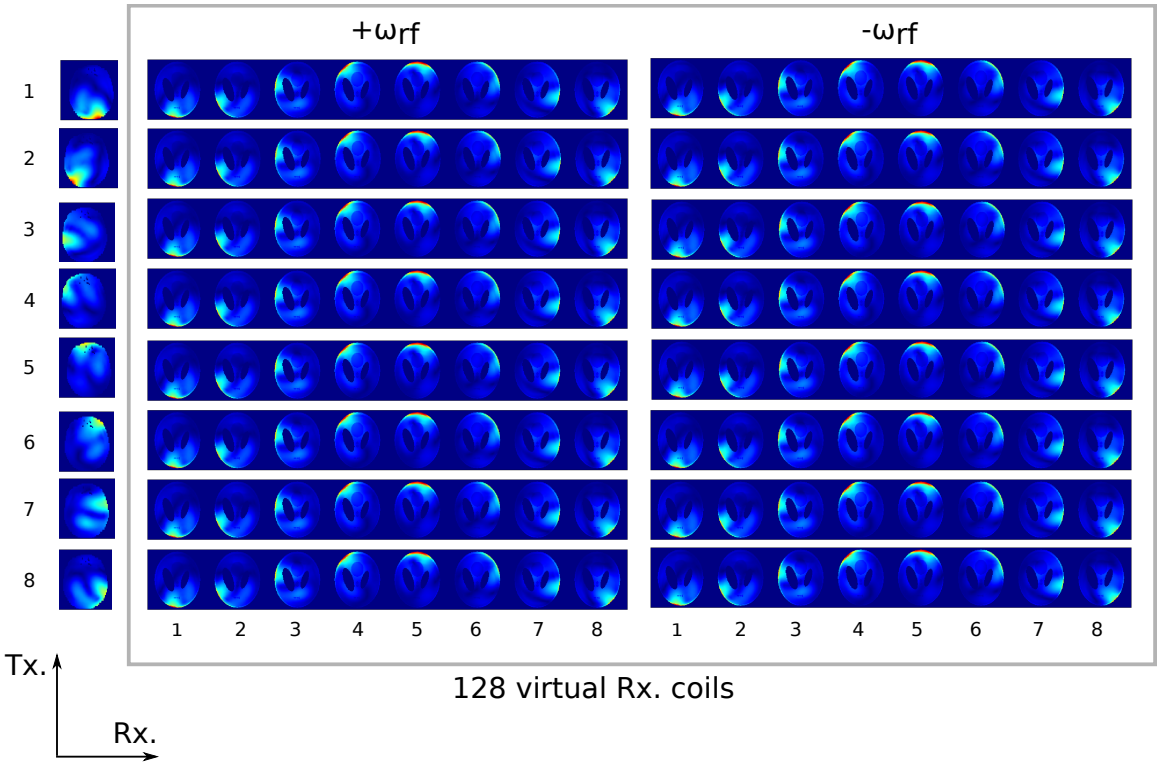

Figure II.1: The central idea of the method. Each BS pulse imparts a unique phase shift pattern to the same underlying image. This fact can be exploited to generate an augmented set of virtual receive coils. In this example, 8 transmit and 8 receive coils with 2 BS encoding pulses give a set of 128 virtual receive coils.

BS $|B_1^+|$ mapping is an inherently fast method if SAR is not a limitation and off-resonance RF pulses with high enough amplitudes can be used to generate detectable phase shifts. Previously, BS acquisitions have been accelerated using single-shot readouts [12]. Compressed sensing has also been applied to magnitude-based $|B_1^+|$ mapping methods [2].

Here we propose a PI approach for Bloch-Siegert (BS) $|B_1^+|$ mapping that allows very

high acceleration factors. The method makes use of the fact that each BS pulse imparts a unique phase shift pattern to the same underlying image, enabling a joint autocalibrated PI reconstruction across all BS acquisitions for a transmit array. Also, since the data for the different transmit coils and off-resonance frequencies are acquired at different times, reconstructions can be improved by acquiring data on disjoint k-space sampling patterns across the transmit coils. The method is shown to produce accurate field maps, in some cases at scan accelerations beyond the number of physical receive coils. The noise performance of this method is quantified by empirically measuring the g-factor and angle-to-noise (ANR) maps in simulations. Additionally, phantom TEM array and head birdcage dual transmit $|B_1^+|$ mapping experimental results at 7 T are shown, to demonstrate the performance of the approach in vivo.

II.2 Theory

As described in Section I.1, Parallel imaging methods perform scan acceleration by skipping k-space lines, and implicitly or explicitly filling in the missing k-space data by exploiting the spatial encoding provided by the coil sensitivities. The more receive coils one has with unique spatial sensitivity patterns, the higher the achievable scan acceleration without major aliasing artifacts. In this work we use this principle to accelerate the $|B_1^+|$ mapping method by generating an expanded virtual coil dataset from the multiple acquisitions in a BS experiment.

Section I.2.2 explained how the BS method uses encoding pulses that cause a change in signal phase depending on the strength of the $|B_1^+|$ field seen by previously-excited magnetization [8]. In multi-transmit-channel BS $|B_1^+|$ mapping, assuming that either the same coil or RF shim is used for each excitation, or, if different coils or shims are used for excitation but T_1 effects can be ignored, then each encoding pulse imparts a unique smooth phase shift to the same underlying image. These phase shifts can be mathematically absorbed into the receive coil sensitivities, leading to an augmented set of virtual receive coils.

The reconstructed image weighted by the receive coil sensitivity can be represented as

$$I_i(\vec{x}) = C_i(\vec{x})M(\vec{x}) \tag{II.1}$$

where I_i is the image for receive coil i, C_i is receive coil i's sensitivity and $M(\vec{x})$ is the transverse magnetization. In BS $|B_1^+|$ mapping, two images are acquired for each transmit coil with the BS pulses at opposite off-resonance frequencies, so that background and B_0 phase can be removed using a phase difference. The image for receive coil i, off-resonance frequency j, and transmit coil k is

$$I_{ijk}(\vec{x}) = C_i(\vec{x})M_{jk}(\vec{x}), \tag{II.2}$$

where M_{jk} is given by

$$M_{jk}(\vec{x}) = M(\vec{x})e^{\imath\phi_{jk}^{BS}(\vec{x})} \tag{II.3}$$

and $\phi_{jk}^{BS}(\vec{x})$ is the BS phase shift, which is approximately proportional to $|B_1^+|^2$. The phase shifts can be absorbed into receive coil sensitivities

$$\begin{aligned} I_{ijk}(x,y) &= [C_i(\vec{x})e^{\imath\phi_{jk}^{BS}(\vec{x})}]M(\vec{x}) \\ &= C_{ijk}(\vec{x})M(\vec{x}) \end{aligned} \tag{II.4}$$

where C_{ijk} is an element of an augmented set of $N_r \times 2 \times N_t$ virtual receive channels, where N_r is the number of physical receive coils, and N_t is the number of transmit coils that are mapped. Thus, BS data for N_t transmit channels, each comprising data for N_r receive channels at two symmetric off-resonant frequencies (+/-), effectively comprises data from $N_r \times 2 \times N_t$ virtual receive channels. We exploit this augmented receive channel array to accelerate BS $|B_1^+|$ mapping beyond the factors that can be achieved using only physical receive coils for acceleration. Furthermore, since the $2 \times N_t$ BS datasets are acquired at different time points, we have the opportunity to improve image reconstruction quality by

acquiring disjoint/staggered k-space sampling patterns for each BS frequency polarity and transmit channel.

II.3 Methods

To demonstrate the broad applicability of the proposed approach, both (Cartesian) GRAPPA [3] and (Cartesian and non-Cartesian) SPIRiT [4] methods were used for the following simulated and experimental autocalibrated PI reconstructions. Both methods require little modification to allow distinct k-space sampling patterns for each receive channel. Three acquisition and reconstruction scenarios were compared to fully-sampled reconstructions in simulations and experiments: (1) Low resolution reconstruction of each of the $2 \times N_t$ BS datasets, where the total number of data points sampled equalled the total number of samples for the accelerated cases; (2) Accelerated independent reconstruction of each of the $2 \times N_t$ BS datasets with the same sampling pattern, exploiting only the physical receive coils for acceleration ('independent'); (3) Joint reconstruction of all $2 \times N_t$ datasets with the same sampling pattern ('joint; same'). (4) Joint reconstruction with staggered sampling across off-resonance frequencies and transmit coils ('joint; staggered'). Acceleration was performed by retrospectively undersampling simulated and measured k-space data. To qualitatively evaluate the quality of magnitude reconstructions, for each transmit channel all the receive channel images were combined as the root of the sum of squares (SoS) of all the individual receive coil images. $|B_1^+|$ maps were estimated from each reconstruction using an image magnitude-weighted average across receive channels as follows

$$|B_1^+|_k = \sum_{i=1}^{N_c} \left[\frac{|I_{i1k}| + |I_{i2k}|}{2} \sqrt{\frac{\angle(I_{i1k} I_{i2k}^*)}{2K_{BS}}} \left(\sum_{i=1}^{N_c} \frac{|I_{i1k}| + |I_{i2k}|}{2} \right)^{-1} \right] \tag{II.5}$$

where $|B_1^+|_k$ represents the $|B_1^+|$ map for transmit coil k, I_{i1k}, I_{i2k} are the reconstructed images for the two BS off-resonant frequencies for receive coil i and transmit coil k. K_{BS} is a constant that describes the phase shift in radians/Gauss^2 for a given BS pulse [8].

All reconstructions were implemented in MATLAB (MathWorks Inc., Natick, MA,

USA). SPIRiT and GRAPPA reconstructions were performed using the image reconstruction library provided by Lustig et al [4], wherein non-uniform fast Fourier transforms were performed using the algorithm in Ref. [13].

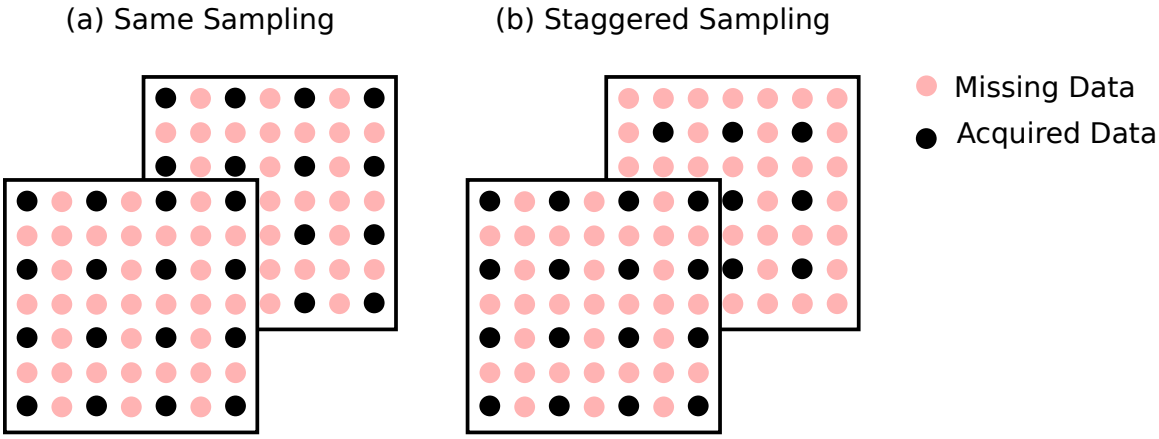

Figure II.2: Staggered Cartesian sampling illustration showing k-space sampling patterns for 2 coils with $4\times$ acceleration. a: The same k-space points are sampled for each transmit coil and Bloch Siegert frequency polarity. b: Disjoint k-space locations are sampled for different transmit coils and frequency polarities.

Figure II.2 illustrates example Cartesian k-space sampling patterns for 'same' and 'staggered' cases. In the same sampling pattern the same k-space location is sampled for each transmit coil. In staggered sampling the k-space locations skipped in one coil are sampled in another coil. The fully sampled calibration region at the center of k-space remains unchanged for the same and staggered patterns.

For the non-Cartesian staggered reconstruction, the single shot spiral trajectory was rotated in increments of $2\pi/(2\times N_t)$ radians to generate a disjoint set of spiral co-ordinates for the extended $2\times N_t$ coil data.

Figure II.3(a) shows an illustration of a dual density sampling scheme for 2 coils at $2\times$ acceleration used in simulations. Figure II.3(b) shows a staggered sampling scheme using multi-shot spiral trajectory used in in-vivo experiments. The spiral k-space co-ordinates are chosen such that all the coils have the same acceleration and each coil has a unique sampling trajectory.

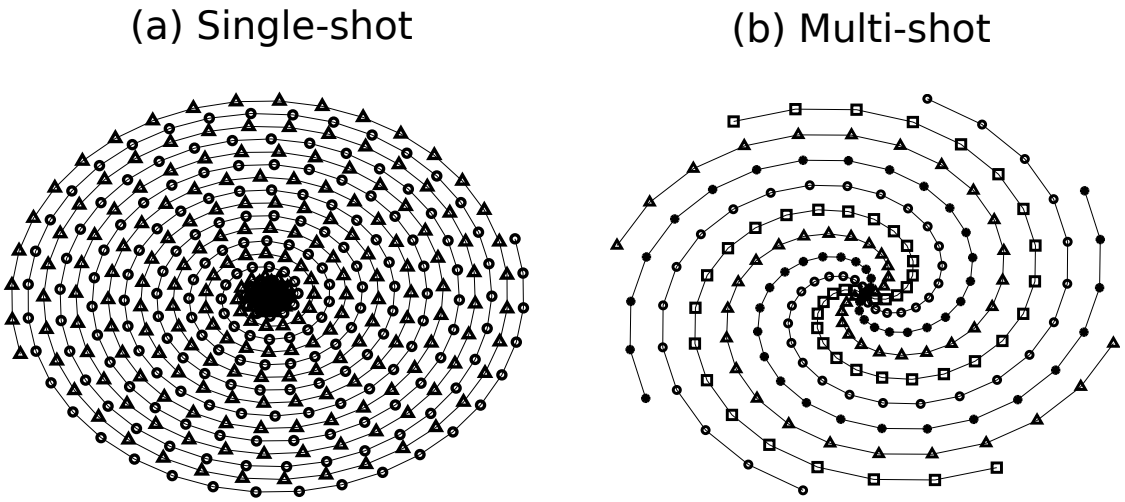

Figure II.3: Illustration of staggered single-shot variable density and multi-shot spiral sampling schemes showing k-space sampling locations for 2 and 4 coils respectively. Each transmit coil and Bloch Siegert frequency polarity is represented by a unique line marker.

II.3.1 Simulations

Simulated BS $|B_1^+|$ mapping data were synthesized from B_1^+ and B_1^- maps calculated using CST Microwave Studio (CST AG, Darmstadt, Germany) at 300 Mhz (7 T) for an 8-channel transmit/receive TEM array in a human head model. The maps had a 24 cm FOV and 128 $\times$128 matrix size. To generate complex BS images with contrast, for each transmit coil a Shepp-Logan phantom was weighted by the B_1^- maps for each receive coil and a BS phase of $\pm\kappa_{BS}|B_1^+(\vec{x})|^2$ was applied, where κ_{BS} is the phase coefficient of a Fermi pulse with duration 8 msec and off-resonance frequency 4 kHz [8]. Cartesian k-space data were generated using Fast Fourier Transforms. Subsequently, GRAPPA reconstruction was performed at 16$\times$ acceleration. A GRAPPA kernel size of 5$\times$5 was chosen with a kernel calibration regularization parameter of 0.01 [4]. To synthesize spiral k-space data the Cartesian data were resampled to a single shot variable density spiral trajectory with a 9 ms readout duration (Fig. II.3a). The center of k-space was fully sampled up to a resolution of 7.35 cm and the 6$\times$ acceleration was used beyond that. The images were reconstructed using image-based non-uniform SPIRiT. Calibration data of size (32$\times$32) were obtained from the fully sam-

pled Cartesian dataset and used to calibrate kernels of size 5×5. The calibration Tikhonov regularization parameter was 0.02, the SPIRiT regularization parameter was 100, and 100 conjugate gradient (CG) iterations were performed. In addition to evaluating image and $|B_1^+|$ reconstruction accuracy, g-factor and angle-to-noise ratio (ANR) maps were determined empirically using Monte Carlo simulations with 100 realizations, wherein complex white Gaussian noise was added to the k-space data.

II.3.2 Experiments

II.3.2.1 Phantom

To validate the method with several transmit channels, phantom data was acquired using a mineral oil phantom on a Philips Achieva 7 T scanner (Philips Healthcare, Cleveland, Ohio) with an in house-built 6-element TEM coil. A gradient echo BS pulse sequence was used with a 2 ms optimized BS pulse [11] for both phantom and in-vivo exams. TE/TR was set to 7.5/500 ms with nominal excitation flip angle of 70 degrees. Cartesian Bloch-Siegert acquisitions were performed with a 25 cm FOV, 256×256 matrix size, and 5 mm slice thickness. Cartesian SPIRiT reconstruction was performed at 16× acceleration with the calibration and reconstruction Tikhonov regularization parameters set to 0.01 and 10^{-5} respectively. Calibration data of size 20×20 were used to calibrate kernels of size 5×5. Thirty CG iterations were performed. To reduce the effects of noise due to poor receive sensitivity, all maps were refined using a penalized-likelihood algorithm [14], which was initialized by first order polynomial fits to the maps.

II.3.2.2 In vivo

To validate the method in vivo, human studies were conducted with the approval of the Institutional Review Board at Vanderbilt University. Data were acquired with a 32 channel SENSE volume coil (Nova Medical Inc., Wilmington, MA), and a 2-channel parallel transmit birdcage coil. 2D single-slice Cartesian and spiral BS data were acquired with a 24 cm FOV, 120×120 matrix size, and a 2 mm slice thickness. TE/TR were set to 12/616 ms

with nominal excitation flip angle of 70 degrees. This setup gave a total of 128 ($2\times32\times2$) augmented virtual receive coils for the joint reconstructions. In all acquisitions the same excitation pulse was used, with the two channels of the birdcage coil driven in quadrature; the transmit channel not being mapped was turned off only during the BS pulse. Cartesian SPIRiT reconstruction was performed at $32\times$ acceleration with the calibration and reconstruction Tikhonov regularization parameters set to 0.01 and 10^{-5} respectively. Calibration data of size 20×20 were used to calibrate kernels of size 5×5. Thirty CG iterations were performed. Spiral data were acquired on a uniform density multi-shot spiral trajectory with 64 interleaves as illustrated in Figure II.3(b). The dataset was retrospectively undersampled by a factor of $8\times$ by dropping interleaves. For comparison with joint reconstructions, a fully-sampled low resolution dataset was generated by truncating the eight uniformly-spaced shots down to the point at which they were fully-sampled, which was defined as the time point at which the distance between adjacent shots was FOV^{-1}. This way, the low-resolution reconstruction used the same number of shots, and thus approximately the same sequence duration as the accelerated acquisition. The reconstruction was performed using non-Cartesian SPIRiT at $8\times$ acceleration with the calibration and reconstruction Tykhonov regularization parameters set to 0.01 and 10^4 respectively. Calibration data of size 32×32 was used to calibrate kernels of size 7×7. Four hundred CG iterations were performed.

II.4 Results

II.4.1 Simulations

II.4.1.1 Cartesian GRAPPA

Figure II.4 shows the $16\times$ accelerated reconstruction images of one of the transmit channels. Despite an acceleration factor of twice the number of receive channels, the jointly-reconstructed $|B_1^+|$ maps contain only small errors, while the independent image and map contain large aliasing artifacts, and the low resolution image and map contain large ringing artifacts. The $|B_1^+|$ maps of the joint; staggered reconstruction closely match the true maps,

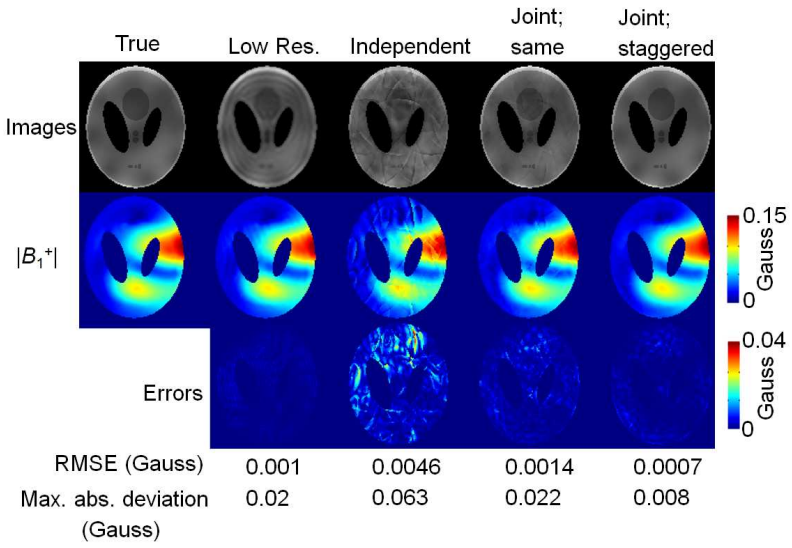

Figure II.4: 16×-accelerated Cartesian sum-of-squares (SoS) images and $|B_1^+|$ map of 1 transmit coil. Joint reconstruction with staggered sampling achieves lowest error.

with the smallest error.

II.4.1.2 Non-Cartesian SPIRiT

Figure II.5 shows the spiral 6× acceleration results. The independent and joint; same images contain large spiral aliasing artifacts, which are not present in the joint; staggered image, though, interestingly, the joint; same $|B_1^+|$ map contains low artifacts. The jointly reconstructed $|B_1^+|$ maps both have an order of magnitude lower error than the independent case, and the joint; staggered $|B_1^+|$ map is the most accurate.

II.4.1.3 Noise Performance

Figure II.6 shows that the joint; staggered reconstruction achieves the smallest maximum noise amplification with the most uniform g-factor for the Cartesian acquisition. The g-factor map for the joint; same reconstruction shows higher noise amplification than both the independent and joint; staggered reconstructions. Interestingly, while the jointly-reconstructed magnitude images have higher noise amplification, the jointly-reconstructed $|B_1^+|$ maps have a higher angle-to-noise (ANR) compared to the independent reconstruc-

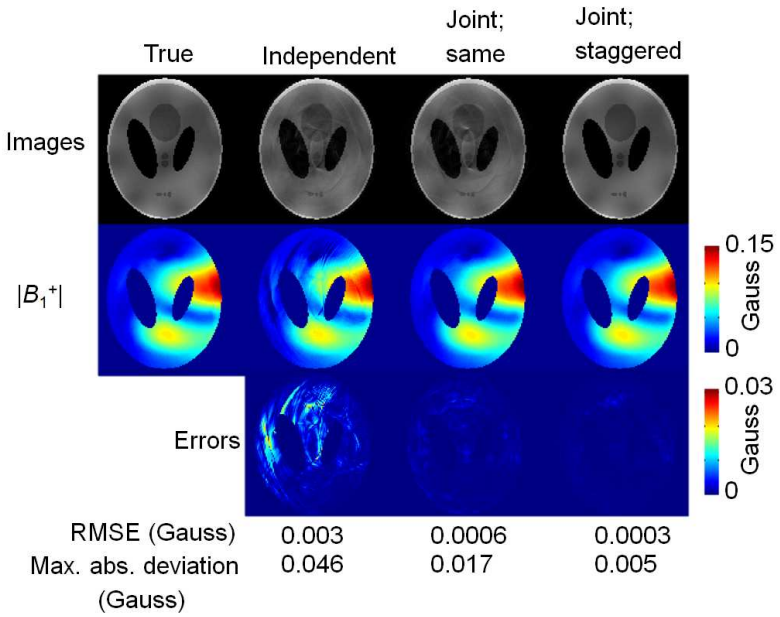

Figure II.5: 6×-accelerated Spiral SoS images and $|B_1^+|$ maps of 1 transmit coil. Joint; staggered reconstruction achieves lowest error.

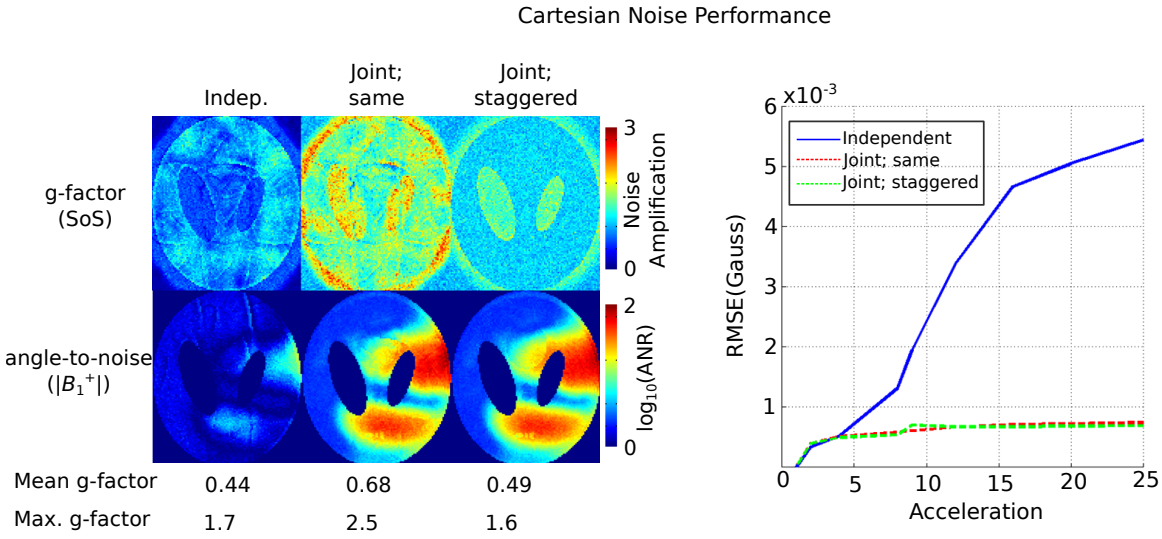

Figure II.6: g-Factor, angle-to-noise (ANR) maps (16× acceleration) and $|B_1^+|$ RMSE vs acceleration. Joint reconstruction with staggered sampling achieves the most uniform g-factor (calculated from SoS magnitude images). Overall, joint reconstructions achieve higher $|B_1^+|$ ANR than independent and their error is relatively flat up to a high acceleration factor.

tion. The root mean square error (RMSE) vs acceleration plot shows that the joint reconstructions have a stable RMSE up to an acceleration factor beyond the number of receive channels, up to a factor of 25×, whereas the independent reconstruction's RMSE rises steeply. Note that the acceleration limit of 25× is imposed by the size of the GRAPPA kernel used for reconstruction, and that it is expected that the joint reconstructions' RMSE would rise steeply at a higher acceleration than was simulated here.

II.4.2 Experiments

II.4.2.1 Phantom Cartesian SPIRiT

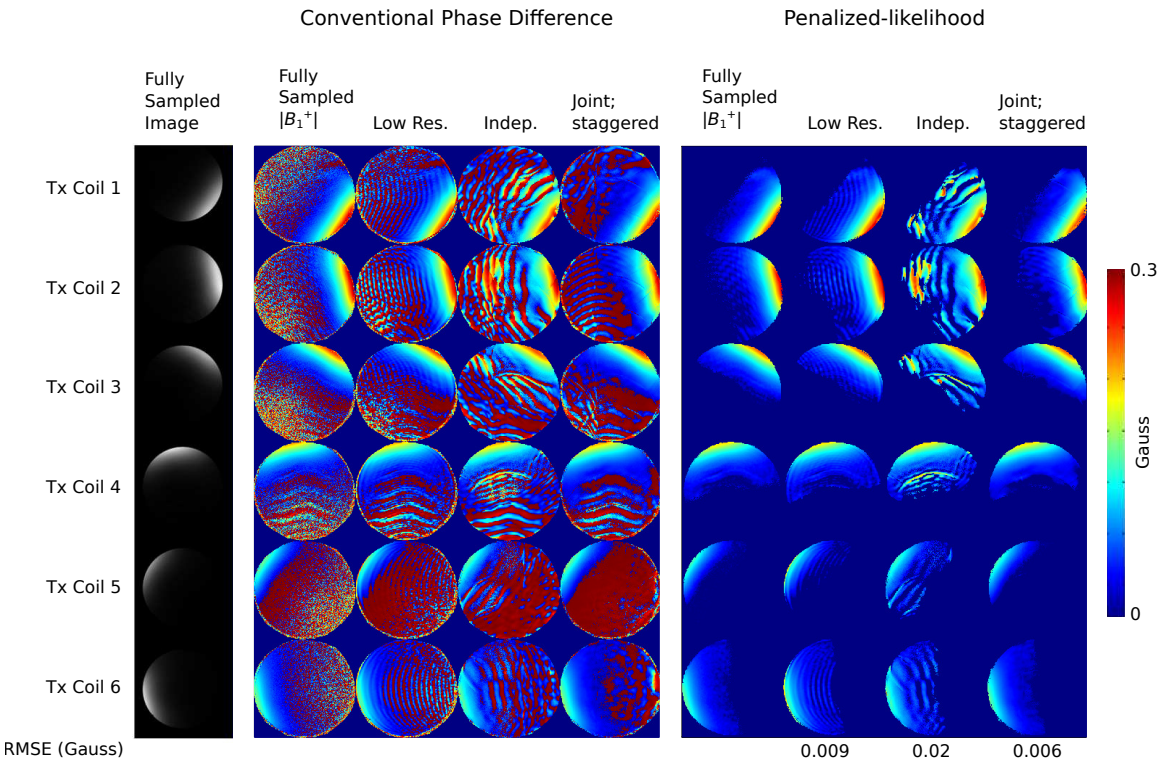

Figure II.7: 16×-accelerated $|B_1^+|$ maps using a 6 channel TEM array coil. Results with conventional phase difference and penalized-likelihood refinement are shown. The joint; staggered reconstruction is most accurate. Note that $N_r = 1$ here.

Figure II.7 shows the results from the 6 transmit-channel phantom $|B_1^+|$ mapping experiment. The joint; staggered maps closely match the fully-sampled maps, while the independently-reconstructed maps have severe aliasing and the low resolution reconstruc-

tion contain ringing artifacts.

II.4.2.2 In Vivo Cartesian SPIRiT

Figure II.8 shows the results from the Cartesian in vivo study. The data were undersampled by a factor of 32×. The joint; staggered magnitude image appears closest to the fully-sampled magnitude. The $|B_1^+|$ maps for the joint reconstructions look very similar and closely match the fully-sampled $|B_1^+|$ maps. In comparison, the independent maps are noisier and contain aliasing artifacts. The low resolution maps are blurred and contain large ringing artifacts.

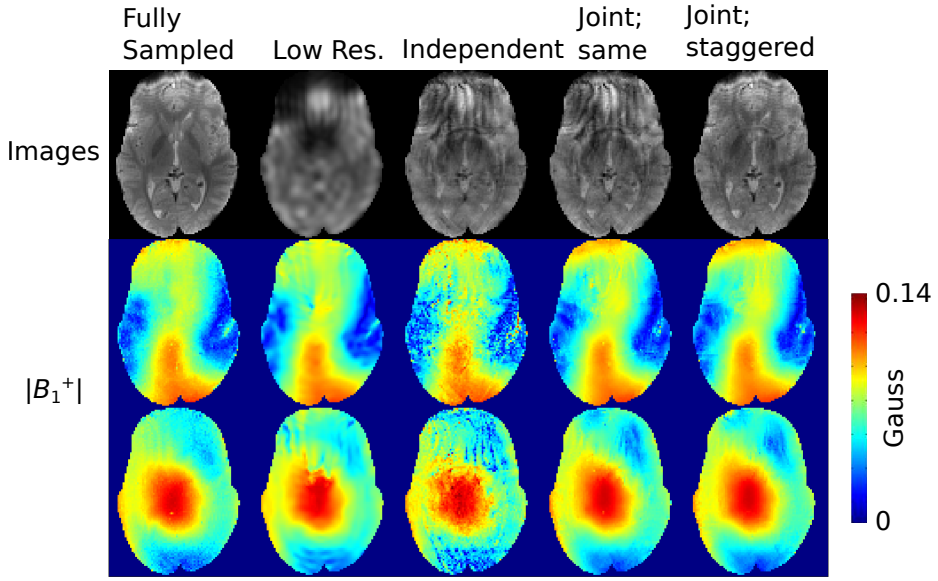

Figure II.8: 32×-accelerated SoS images and $|B_1^+|$ maps of 2 transmit coils. The joint; staggered reconstruction is most accurate. $N_r = 32$ here.

II.4.2.3 In Vivo Non-Cartesian SPIRiT

Figure II.9 shows the non-Cartesian in vivo reconstructions. Again, the joint; staggered reconstruction produced the closest magnitude image to the fully-sampled reconstruction. Most of the ringing artifacts seen in the independent and joint; same images do not appear in the joint; staggered image. The low resolution $|B_1^+|$ maps are oversmoothed, and the

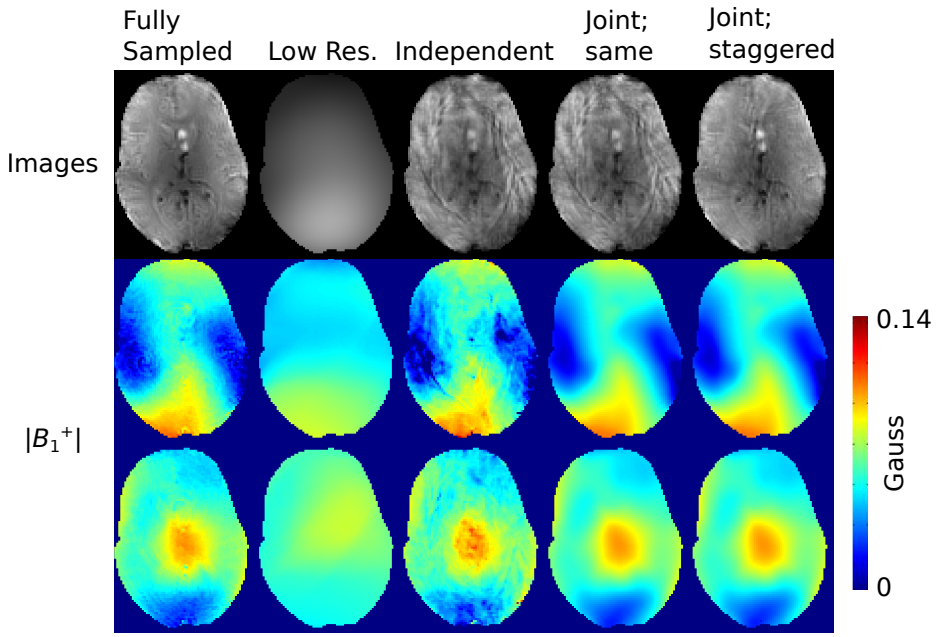

Figure II.9: 8×-accelerated SoS images $|B_1^+|$ maps of 2 transmit coils. The joint; staggered reconstruction is most accurate. $N_r = 32$ here.

independent maps show higher noise levels and aliasing artifacts. In contrast, the $|B_1^+|$ maps for the joint reconstructions closely match the fully-sampled maps.

II.5 Discussion

We have presented a simple approach to accelerate Bloch-Siegert $|B_1^+|$ map acquisition without sacrificing accuracy. The method was shown to apply to both Cartesian and non-Cartesian data using two different autocalibrating parallel image reconstruction methods. It can also be used in single transmit systems to jointly reconstruct the images for the two off-resonance frequencies in a BS acquisition. More broadly, the general approach of jointly reconstructing $|B_1^+|$ mapping images across transmit coils may be applicable to many $|B_1^+|$ mapping methods, though T_1 relaxation would be a concern for magnitude-based methods such as AFI [15] and double angle [16].

The proposed approach is expected to benefit tailored parallel excitation which requires acquisition of multiple transmit channels. Though it is typical in parallel excitation to

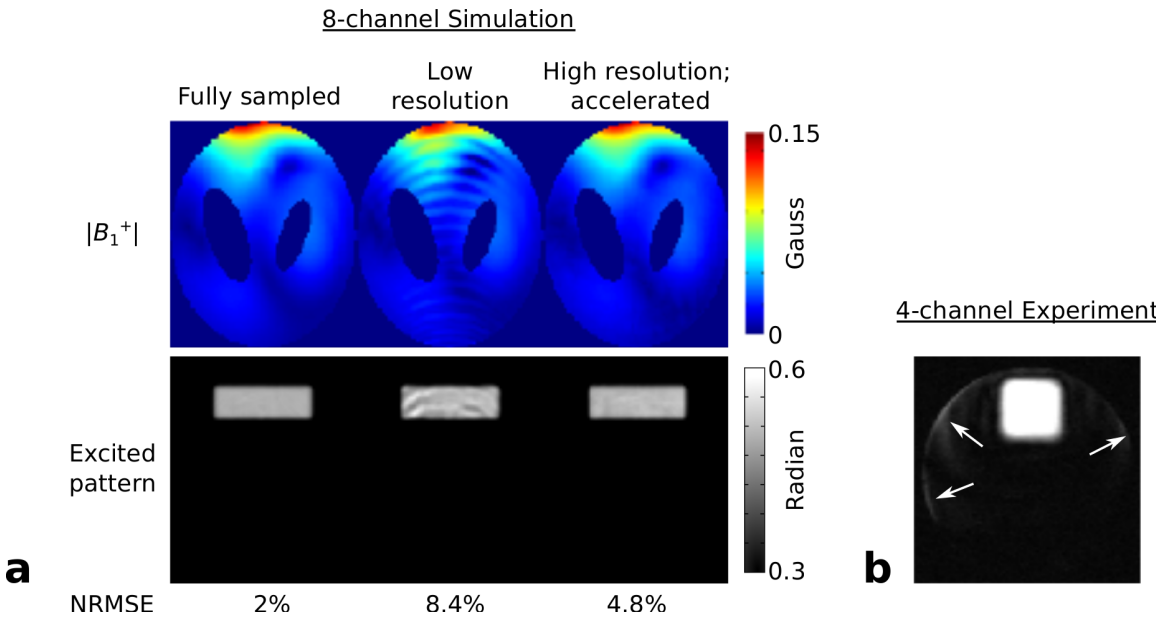

Figure II.10: a: Simulation of erroneous excitation in 8-channel, 6×-accelerated spiral parallel excitation designed using low resolution $|B_1^+|$ maps. Ringing artifacts in the passband are alleviated by pulses designed with $|B_1^+|$ maps reconstructed at a high resolution, using the proposed method to accelerate $|B_1^+|$ acquisition and achieve a scan time equivalent to a low-resolution acquisition. b: Erroneous excitation in 4 coils, 2×-accelerated parallel transmit, due to partial volume effects at object edges in $|B_1^+|$ maps, [1]. The excitation errors are ∼18% of the peak flip angle.

use $|B_1^+|$ maps of lower resolutions (64×64 matrix sizes are common) than we acquired here, such low resolutions can lead to excitation errors in the designed pulses. This is because the body effectively masks $|B_1^+|$ maps, introducing sharp boundaries that result in ringing artifacts throughout the maps, and/or partial volume effects at those boundaries. While this is not a significant problem for RF shimming, it can significantly degrade the performance of parallel excitation pulses with relatively high spatial resolution, such as pulses for reduced-FOV imaging, as is demonstrated in Fig. II.10. The proposed method enables rapid acquisition and accurate reconstruction of high resolution maps with reduced excitation errors.

CHAPTER III

CONCLUSIONS

The research work reported in this thesis has presented a novel approach to accelerate the Bloch-Siegert transmit RF field map reconstructions. The extra encoding provided by the BS pulses was utilized to create a set of virtual receive coils, which allowed higher acceleration factors in autocalibrating parallel image reconstructions. The proposed method is shown to give good quality $|B_1^+|$ maps at high accelerations for both uniform and non-uniform k-space sampling, using two different parallel image reconstruction methods. It is a simple approach to accelerate $|B_1^+|$ map acquisitions that exploits the extra degrees of freedom inherently provided in a typical BS experimental set-up, and does not require gathering any additional data. However, the method does have some drawbacks, especially when used with iterative image reconstruction methods. Most iterative methods require tuning parameters such as the Tikhonov regularization factor in SPIRiT. These parameters may need to be manually set on a case-by-case basis. Another drawback is that for a large number of virtual receive coils, iterative methods may become time consuming if the implementation doesn't use a computationally-efficient algorithm.

The method is expected to be most useful for parallel excitation and RF shimming applications, where it is desirable to rapidly measure $|B_1^+|$ maps of many transmit coils during a prescan stage. $|B_1^+|$ inhomogeneity is a substantial problem in high and ultra high field imaging. Therefore patient tailored RF pulse design methods are used to generate pulses that compensate for field inhomogeneity unique to each subject. Since the $|B_1^+|$ mapping procedure has to be repeated for each subject, the proposed method will benefit in accelerating patient tailored imaging.

BIBLIOGRAPHY

[1] Stang P, Kerr A, Pauly JM, and Scott G. An extensible transmit array system using vector modulation and measurement. *In: Proceedings of the 16th Annual Meeting of ISMRM, Toronto, Ontario, Canada*, page 145, 2008.

[2] Doneva M, Nehrke K, Mertins A, and Börnert P. Compressive B_1^+ mapping: Towards faster transmit coil sensitivity mapping. *In: Proceedings of the Joint Annual Meeting ISMRM-ESMRMB, Stockholmsmassan AB, Stockholm, Sweden*, page 2833, 2010.

[3] Griswold MA, Jakob PM, Heidemann RM, Nittka M, Jellus V, Wang J, Kiefer B, and Haase A. Generalized autocalibrating partially parallel acquisitions (GRAPPA). *Magn Reson Med*, 47(6):1202–1210, 2002.

[4] Lustig M and Pauly JM. SPIRiT: Iterative self-consistent parallel imaging reconstruction from arbitrary k-space. *Magn Reson Med*, 64(2):457–471, 2010.

[5] PB Roemer, WA Edelstein, CE Hayes, SP Souza, and OM Mueller. The nmr phased array. *Magnetic resonance in medicine*, 16(2):192–225, 2005.

[6] Klaas P Pruessmann, Markus Weiger, Markus B Scheidegger, Peter Boesiger, et al. Sense: sensitivity encoding for fast mri. *Magnetic Resonance in Medicine*, 42(5):952–962, 1999.

[7] Daniel K Sodickson and Warren J Manning. Simultaneous acquisition of spatial harmonics (smash): fast imaging with radiofrequency coil arrays. *Magnetic Resonance in Medicine*, 38(4):591–603, 2005.

[8] Sacolick LI, Wiesinger F, Hanc I, and Vogel MW. B_1 mapping by Bloch-Siegert shift. *Magn Reson Med*, 63(5):1315–1322, 2010.

[9] F Bloch and A Siegert. Magnetic resonance for nonrotating fields. *Physical Review*, 57(6):522, 1940.

[10] Norman F Ramsey. Resonance transitions induced by perturbations at two or more different frequencies. *Physical Review*, 100(4):1191, 1955.

[11] Jankiewicz M, Gore JC, and Grissom WA. Improved encoding pulses for Bloch-Siegert B_1^+ mapping. *J Magn Reson Imaging*, 226:79–87, 2012.

[12] Khalighi MM, Glover GHP, Pandit SH, Kerr AB, Saranathan A, and Rutt BK. Single-shot spiral based Bloch-Siegert B_1^+ mapping. *In: Proceedings of the 19th Annual Meeting of ISMRM, Montreal, Quebec, Canada*, page 578, 2011.

[13] Fessler JA and Sutton BP. Nonuniform fast Fourier transforms using min-max interpolation. *IEEE Trans Signal Processing*, 51(2):560 – 574, feb 2003.

[14] Zhao F, Fessler JA, Nielsen J, Yoon D, and Noll DC. Regularized estimation of magnitude and phase of multiple-coil B_1 field via Bloch-Siegert B_1 mapping. *In: Proceedings of the 20th Annual Meeting of ISMRM, Melbourne, Victoria, Australia.*, page 2512, 2012.

[15] Yarnykh VL. Actual flip-angle imaging in the pulsed steady state: A method for rapid three-dimensional mapping of the transmitted radiofrequency field. *Magn Reson Med*, 57:192–200, 2007.

[16] Insko EK and Bolinger L. Mapping of the radiofrequency field. *J Magn Reson Imaging*, 103:82–85, 1993.